The 11th International Topical Meeting on Nuclear Reactor Thermal-Hydraulics (NURETH-11)
Popes' Palace Conference Center, Avignon, France, October 2-6, 2005.

SONOFUSION – FACT OR FICTION?

Richard T. Lahey, Jr.[1]
Rensselaer Polytechnic Institute
Troy, NY 12180-3590 USA
laheyr@rpi.edu
+1(518) 276-6614

Rusi P. Taleyarkhan
Purdue University
West Lafayette, IN 47907 USA
rusi@purdue.edu

Robert I. Nigmatulin
Russian Academy of Sciences
Ufa, Bashkortostan 450077 Russia
nigmar@anrb.ru

ABSTRACT

Sonoluminescence and Sonofusion phenomena may occur when vapor bubbles implode. This paper reviews the status of our understanding of the bubble dynamics involved in these interesting phenomena. In particular, the experimental and analytical evidence supporting the observed production of neutrons and tritium due to thermonuclear fusion within imploding bubble clusters is reviewed. Moreover, potential methods to scale-up the neutron yield and some potential applications of this exciting new technology are discussed.

INTRODUCTION

Bubble dynamics is a large and interesting topic in the field of multiphase flow and heat transfer. An important subset of this topic has to do with Sonoluminescence and Sonofusion technology, and the latter will be the main focus of this paper. It should be noted that we will be concerned with the creation of conditions during the implosion of cavitation bubbles which are suitable for thermonuclear fusion (i.e., ultra-high temperatures, pressures and densities) rather than the conditions normally associated with "cold fusion." Indeed, the physics of Sonofusion is that of thermonuclear fusion, and thus is quite different from any "new" physics which may be associated with "cold fusion."

Let us begin with a review of Sonoluminescence. This is a phenomena in which light pulses are observed during ultrasonically-forced gas/vapor bubble implosions. This

[1] Corresponding Author

phenomena has been known for more than 70 years [Marinesco & Trillat, 1933], [Frenzel & Schultes, 1934], [Zimakov, 1934] and it has been widely used by chemists in Sonochemistry.

Many different theories have been advanced to explain Sonoluminescence, but most researchers now agree that the observed light pulses are due to shock wave heating of the highly compressed gas/vapor to incandescent temperatures.

Figure-1 is a schematic of an imploding gas/vapor bubble. Figure-1a shows the bubble being compressed by the surrounding liquid which is at a higher pressure. At this point in time the Mach number of the interface $\left(\mathrm{Ma}_g = \left|\dot{\mathrm{R}}\right| / \mathrm{C}_g\right)$ is less than unity, and thus no shock waves are formed within the bubble. Figure-1b shows a later time at which $\mathrm{Ma}_g \geq 1$ and a spherical shock wave has been formed. This shock wave significantly strengthens as it converges to the center of the bubble. Figures 1c and 1d show situations just after the shock wave has bounced off itself at the center of the bubble. This process leads to very high local pressures and temperatures, and the emission of a visible light pulse, and if the compressed material and conditions are suitable, nuclear (i.e., neutron) emissions. Figures 1e and 1f show subsequent times in which a rarefying shock wave travels outward from the bubble, which is now expanding because the pressure in the surrounding liquid has been reduced.

Sonoluminescence has a very large literature associated with it, for both multiple bubble sonoluminescence (MBSL) and single bubble sonoluminescence (SBSL). This interesting field has been well summarized [Crum, 1994], [Lauterborn et al, 1999], [Putterman & Weininger, 2000], [Margulis, 2000], [Young, 2004], and thus it will not be considered in detail in this paper. Suffice it to say that it has been found that during SBSL, in which a single gas bubble is levitated in the antinode of a standing pressure field and it repetitively expands and implodes at the externally-imposed ultrasonic frequency of the pressure field, that there are some inherent limitations on how energetically the bubble can be imploded. These limitations are due to shape/interfacial instability mechanisms, rectified diffusion, endothermic chemical reactions, and the so-called Bjerknes force, $-\left\langle \mathrm{V}(\mathrm{t})\nabla \mathrm{p}(\mathrm{t})\right\rangle$, which can entrap the bubble in the acoustic anti-node, and reverses sign during acoustic pressure amplitudes over about 1.7 bar [Akhatov et al, 1997]. These limitations appear to be fundamental and limit the measured [Camera et al, 2004] and predicted [Moss et al, 1994; 1996; 1997] peak gas/plasma temperatures to about 10^6 K.

In any event, it was recognized early-on by the authors of this paper, that in order to be able to achieve conditions suitable for thermonuclear fusion that a completely different experimental approach was required. In particular, a technique which was originally developed for neutron detection [West et al, 1967; 1968; 1969] was adapted for our Sonofusion experiments [Taleyarkhan et al, 2002; 2004].

In contrast to typical SBSL experiments, in which non-condensable gas bubbles are repeatedly imploded, in Sonofusion experiments the liquid is well-degassed and cavitation vapor bubbles are created and imploded.

It is important that the test liquid contain materials that can undergo thermonuclear fusion (e.g., deuterium, D, or tritium, T), and that it be able to withstand significant tension without undergoing premature cavitation. Fortunately, many organic liquids, such as hydrocarbons, satisfy this requirement.

The essence of the experimental technique used in Sonofusion experiments is shown schematically in Figure-2. It can be seen that the well-degassed liquid is put into tension (i.e., at a pressure well below a perfect vacuum) in the antinode of a standing pressure wave. At the minimum pressure, an external neutron source (e.g., a pulse neutron generator, PNG) is activated, and some of the high energy neutrons emitted interact with the highly tensioned liquid, causing it to cavitate and form a bubble cluster. Since the liquid is highly superheated, it evaporates quickly, causing the vapor bubbles to grow rapidly until the externally-impressed harmonic pressure field becomes positive, which causes the bubbles to implode. As noted previously, in connection with figure-1, this sudden collapse of the bubbles will cause them to emit SL light flashes (which can be easily detected with a photomultiplier tube, PMT), and if the test liquid and conditions are suitable, fusion neutrons (which can be detected using a suitable liquid (LS) scintillator). Subsequently a rarefying shock wave in the liquid will reach the test section wall, where it can be easily heard and detected.

It should be noted in typical SBSL experiments the gas bubbles grow from an equilibrium radius, R_o, to, $R_{max_{SBSL}} / R_o \simeq 10$. In Sonofusion, SF (i.e., bubble nuclear fusion), experiments we have a much stronger implosion (i.e., $\left|\dot{R}_{SF}\right| > \left|\dot{R}_{SBSL}\right|$) and , $R_{max_{SF}} / R_{max_{SBSL}} \sim 10$ (hence, $V_{max_{SF}} / V_{max_{SBSL}} \sim 10^3$). Thus, since the kinetic energy in the liquid which is compressing the bubble is proportional to $R^3\dot{R}^2$, we have a kinetic energy in the liquid which is about 10^4 larger in SF than in SBSL, which implies a much larger internal energy in the compressed vapor/plasma bubbles in SF experiments. Indeed, it is this increase in the liquid's kinetic energy which, when focused within the imploding bubble, gives rise to thermonuclear conditions.

Let us now consider the experimental and analytical findings which support the claims of Sonofusion.

DISCUSSION - EXPERIMENTS

Several seminal Sonofusion experiments were performed at Oak Ridge National Laboratory (ORNL) by Taleyarkhan et al [2002], and detailed confirmatory experiments were subsequently conducted and published by them [Taleyarkhan et al, 2004]. A number of criticisms were raised concerning these startling and important experimental results, and these have now been thoroughly discussed and resolved [Nigmatulin et al,

2004]. Indeed, it appears that even our former strongest critics may have changed their minds about Sonofusion [Mullins, 2005].

The ORNL bubble nuclear fusion (i.e., Sonofusion) experiments were conducted in a cylindrical glass test section to which was attached a ceramic PZT transducer ring. The test section was filled with either well-degassed normal acetone (C_3H_6O) or deuterated-acetone (C_3D_6O) as the test liquids. As can be seen in figure-3, state-of-the-art nuclear instrumentation was installed to measure the fusion neutrons (LS) and light pulses (PMT) which may be emitted during bubble cluster implosions. The external excitation of the PZT ring was coordinated with the external pulsed neutron generator (PNG), so that it would emit a burst (6μs at FWHM) of high energy (14.1 MeV) D/T neutrons when the test liquid was at maximum tension (~ -15 to -40 bar). Subsequently, the sequence of events shown schematically in figure-2 took place.

When chilled (i.e., 0˚C), well-degassed D-acetone was used as the test liquid, an average D/D neutron production rate of about $\dot{n}_n = 4\times10^5$ neutrons/s was measured [Taleyarkhan et al, 2002; 2004]. It is significant that 2.45 MeV D/D fusion neutrons were measured only when chilled, well-degassed, cavitated D-acetone was used. That is, no neutrons were measured when room temperature D-acetone, or as expected, normal acetone, was used.

The D/D fusion reaction has two possible outcomes with about an equal probability (i.e., a unity branching ratio):

$$D + D \rightarrow {}^3He(0.82MeV) + n(2.45MeV)$$

and,

$$D + D \rightarrow T(1.01MeV) + H(3.02MeV)$$

Thus tritium ($T \equiv {}^3H$) measurements were also made to independently confirm the occurrence of D/D fusion [Taleyarkhan et al, 2002; 2004].

The data shown in figure-4 indicates a statistically significant monotonic build-up of tritium for testing in chilled, well-degassed, cavitated D-acetone (but not for any other case). It can be seen that when a Plutonium-Beryllium (Pu-Be) source was used that the production rate of tritium is less (by ~75%) than when the PNG is used. This is because, unlike a PNG neutron source, which is synchronized with the acoustic pressure field, a Pu-Be source emits neutrons at random times which are not always at the point of maximum tension in the test liquid. Thus the creation of energetic bubble cluster implosions is less efficient.

In order to infer the D/D neutron production rate from the tritium data we can take a representative sample ($V_{sample} \simeq 1$ mℓ) of the test liquid, put it into a suitable scillination

cocktail (e.g., ~15 mℓ of Exolite) and count the beta-induced scintillations of the tritium. The count rate of this sample is related to the decay constant (λ) of tritium (T) by:

$$\dot{n}'''_T \equiv \frac{dn'''_T}{dt} = \lambda n'''_T \qquad (1a)$$

where, $\lambda = \ell n 2 / T_{1/2}$

$T_{1/2}$ = 12.36 yrs (for Tritium)

$n'''_T = n_T / V_{sample}$

Assuming a uniform concentration of tritium in the test liquid ($V_{TS} \simeq 450$ mℓ) in the test section (TS), and a unity branching ratio, we have,

$$\dot{n}_n = \dot{n}_T = \dot{n}'''_T V_{TS} \qquad (1b)$$

Applying this process to the measured tritium data [Taleyarkhan et al, 2002; 2004] we have [Nigmatulin et al, 2004], $\dot{n}_n \sim 4 \times 10^5$ neutrons/s (see Fig. 4), which is in good agreement with the D/D neutron rate which was measured. Thus the tritium measurements provide independent confirmation of the D/D neutron measurements.

As discussed previously, figure-2 implies the coincidence of the neutron and SL light signals. Figure-5 presents typical experimental data [Taleyarkhan, 2002] which shows this coincidence and the subsequent occurrence of the rarefying shock wave in the liquid striking the test section wall (i.e., the wall microphone signal).

It is interesting to note in figure-6 that after the first energetic implosion of the bubble cluster that the standing acoustic wave was de-tuned for about ten acoustic cycles (~ 500 μs). Subsequently the pressure field recovers and the cavitation bubble cluster again implodes (i.e., "bounces") at the externally-impressed acoustic frequency, again producing D/D neutrons and coincident SL light signals (see the insert in figure-6 for the cavitation on case). This response is apparently due to the interaction between the initial shock wave with the test section wall [Lahey et al, 2005].

Figure-7 shows the time correlation between the 2.45 MeV D/D neutrons and the subsequent production of 2.2 MeV prompt gamma rays associated with the absorption of D/D neutrons by the hydrogen isotope in the liquid pool. As expected from neutron transport analysis, these gamma rays occur over an interval (~ 10 to 20 μs) after neutron emission during which the D/D neutrons interact with the test liquid [Taleyarkhan, 2005].

As another check on the production of D/D neutrons, figure-8 shows the energy distribution of the measured neutrons [Taleyarkhan, 2004]. As can be seen chilled, cavitated D-acetone produced a very statistically significant (> 26 SD) measurement of neutrons above background for energies at or below 2.45 MeV. This is exactly what

would be expected from the monoenergetic D/D fusion neutrons, due to the way in which these neutrons interact with the external LS detector (see figure-3), structures and test liquid [Knoll, 1989].

DISCUSSION-ANALYSIS

It is convenient to analyze the bubble dynamics of Sonofusion experiments in two distinct regimes. The low Mach number ($Ma_g \leq 0.1$) regime, which occurs during most of the acoustically-forced transient, and the high Mach number regime ($Ma_g > 0.1$) which only occurs during the final stages (~ ns) of the bubble implosion process.

During the low Mach number regime, the bubble dynamics are well described by an extended Rayleigh equation [Nigmatulin et al, 2000],

$$R\ddot{R} + \frac{3}{2}\dot{R}^2 = \frac{\left(p_{\ell_i} - p_I\right)}{\rho_\ell} + \frac{R}{\rho_\ell C_\ell}\frac{d}{dt}\left(p_{\ell_i} - p_I\right) \qquad (2)$$

where the last term on the right hand side of Eq. (2) accounts for acoustic scattering, R(t) is the bubble's radius, p_{ℓ_i} is the interfacial pressure (on the liquid side) and p_I is the incident acoustic pressure at the edge of a compression boundary layer in the liquid pool[Nigmatulin et al, 2000]. Equation (2) can be integrated assuming an isothermal, homobaric model for the vapor and approximate interfacial jump conditions, which account for phase change [Lahey et al, 2005].

When the Mach number, $Ma_g = \left|\dot{R}\right|/C_g$, becomes 0.1, one must switch to a full hydrodynamic shock (i.e., HYDRO) code formulation. Assuming the validity of spherical symmetry[2] the model is:

Mass Conservation Equation (k = v or ℓ)

$$\frac{\partial \rho_k}{\partial t} + \frac{1}{r^2}\frac{\partial}{\partial r}\left(\rho_k u_k r^2\right) = 0 \qquad (3)$$

Momentum Conservation Equation (k = v or ℓ)

$$\frac{\partial \rho_k u_k}{\partial t} + \frac{1}{r^2}\frac{\partial}{\partial r}\left(\rho_k u_k^2 r^2\right) + \frac{\partial p_k}{\partial r} = 0 \qquad (4)$$

[2] The validity of the assumption has been supported by the 3-D DNS results on bubble implosions by Nagrath et al [2005].

Energy Conservation Equation (k = v or ℓ)

$$\frac{\partial e_k}{\partial t}+\frac{1}{r^2}\frac{\partial}{\partial r}\left(u_k r^2\left(e_k+p_k\right)\right)=\frac{1}{r^2}\frac{\partial}{\partial r}\left(k_k r^2\frac{\partial T_k}{\partial r}\right) \tag{5}$$

where the vapor/plasma pressure and internal energy density implicitly contain the effect of the ion, electrons and photons. The importance of each component depends on their respective energy levels.

Equations of State

In order to evaluate these phasic conservation equations, we need equations of state, p = p(ρ,T) and ε = ε (ρ,), which are valid over a wide range of pressures and temperatures.

The Mie-Gruneisen equation of state for a highly compressed fluid is:

$$\varepsilon=\left(e/\rho-u^2/2\right)=\varepsilon_p+\varepsilon_T+\varepsilon_c;\, p=p_p+p_T;\; p_T=\rho\Gamma\left(\rho,T\right)\overline{c}_V T;\; \varepsilon_T=\overline{c}_V\left(\rho,T\right)T \tag{6}$$

Where ε_p and p_p are the potential, or "cold," components and ε_T and p_T are the thermal, or "hot," components of the internal energy and pressure, respectively, ε_c is the "chemical energy" (associated with dissociation and ionization), Γ is the Gruneisen coefficient, and $\overline{c}_V$ is an average heat capacity at constant volume.

The potential, or "cold," components characterize the intermolecular force interactions, which depend on the average distances between the molecules which, in turn, depends on the density, ρ. For rarefied gases, where these distances are very large (i.e., for small densities, ρ), the potential components are negligibly small. In contrast, the potential components (ε_p and p_p) are essential for dense gases (i.e., at very high pressures) and for condensed (liquid and solid) states of matter. The thermal, or "hot," components (ε_T and p_T) are traditional thermodynamic parameters which characterize the internal energy and pressure due to the chaotic thermal motion of the molecules. For many fluids, including acetone, the Gruneisen coefficient, Γ, depends only on density, ρ, (i.e., Γ = Γ(ρ)).

The potential components can be quantified using a Born-Mayer potential:

$$p_p=A\left(\frac{\rho}{\rho_0}\right)^{-a+1}\exp\left[b\left(1-\left(\frac{\rho}{\rho_0}\right)^{-a}\right)\right]+E\left(\frac{\rho}{\rho_0}\right)^{m+1}-K\left(\frac{\rho}{\rho_0}\right)^{n+1}+\Delta p_p, \tag{7a}$$

$$\varepsilon_p=\frac{3A}{\rho_0 b}\exp\left[b\left(1-\left(\frac{\rho}{\rho_0}\right)^{-a}\right)\right]+\frac{E}{m\rho_0}\left(\frac{\rho}{\rho_0}\right)^{m}-\frac{K}{n\rho_0}\left(\frac{\rho}{\rho_0}\right)^{n}+\Delta\varepsilon_p+\varepsilon^0. \tag{7b}$$

where, A, K, E, a, b, m and n are constant coefficients, which completely specify the Born-Mayer potential, and $\Delta\varepsilon_p$ is a correction for potential energy [Nigmatulin et al, 2005]. Using Eqs. (6) and (7), the equation of state (EOS) for D-acetone, and the shock tube data of Trunin et al [1992] is shown in Figure-9. It is important to note that the different phases (e.g., liquid and vapor) of acetone take place only for subcritical conditions. That is, for, $p < p_{cr}$, $T < T_{cr}$.

To stimulate the thermal conductivity of an ionized vapor, k_v, we may write [Zeldovich and Raizer, 1966]:

$$k_v \equiv k_{ii} = a_1 T_v^m + a_2 \tag{8a}$$

The transient heat flux is given by [Tien et al, 1998],

$$\tau_{ii} \frac{\partial q''}{\partial t} + q'' = -k_v \nabla T_v \tag{8b}$$

where m = 0.5 and $\tau_{ii} \sim 10^{-13}$ s [Lahey et al, 2005]. This model is expected to give a reasonable estimate of the transient thermal conductivity of the ionized vapor and the associated heat loss.

During the supercompression of a vapor bubble in a liquid of the same substance, both the liquid and vapor of D-acetone may dissociate, and as can be seen in Figure-9, this will change the EOS. We note that non-dissociated (NDis) liquid D-acetone has a relatively steep slope compared to fully dissociated (Dis) liquid D-acetone. Significantly, it is the non-dissociated EOS that is valid during the rapid transient ($\Delta t << 10$ns) associated with the final stages of the bubble implosion process. That is, significant dissociation of acetone liquid does not occur during the very short time interval associated with an implosion. This implies that the liquid remains "stiff," and this, in turn, implies a stronger shock wave within the imploding bubbles.

A discussion of the modeling of the dynamics of the dissociation, ionization and phase change processes has been given by Nigmatulin et al [2005], and this will not be repeated herein. Suffice it to say that the endothermic "chemical" energy associated with the dissociation and ionization processes amounts to the equivalent of 10^6K to 10^7K. These endothermic reactions thus strongly limit the temperature in SBSL experiments, but not in Sonofusion experiments, where, as will be shown subsequently, this energy requirement is only ~5% of that generated during energetic implosions (i.e., the peak vapor/plasma temperature is at least 10^8 K).

Another observation that is quite important has to do with the electron temperature. Due to the way the shock wave induced ionization process occurs (which is quite different from that in laser induced inertial confinement fusion) the electrons and ions initially have about the same velocity but much different masses. Thus the initial temperature (i.e., kinetic energy) of the electrons is much less than that of the ions. Moreover,

because of the speed of the later stages of the implosion process, the electrons remain at a much lower energy than the ions. Indeed, the energy associated with the electrons can be neglected during the energetic bubble implosions associate with Sonofusion. This means that many of the most important radiation energy loss mechanisms (i.e., bremsstrahlung, line losses, recombination losses, etc.) are negligible. Moreover, the pressures and internal energy densities in Eqs. (4) and (5) are essentially those associated with the ions. This observation greatly simplifies the modeling of the problem, and allows us to sweep all our ignorance into the equations of state, Eqs. (6) and (7), which are based on the shock tube acetone data of Trunin et al [1992].

Nucleation and Bubble Cluster Phenomena

When a high energy neutron (e.g., those emitted by a PNG) interacts with the test liquid which is in tension at the acoustic antinode, it may deposit enough energy to create knock-on ions (i.e., for D-acetone, ions of C, D and O) which, in turn, deposit their kinetic energy into the liquid causing bubble cluster nucleation. Detailed neutron and ion transport simulations have shown [Lahey et al, 2005] that, for the conditions of the ORNL bubble nuclear fusion experiments, about 1,000 cavitation bubbles may be in each bubble cluster, which is consistent with direct experimental observations [Taleyarkhan et al, 2002; 2004].

The fact that we have a bubble cluster (rather than a single bubble) is significant since when the bubble cluster implodes the pressure within the bubble cluster may be greatly intensified [Brennen, 1995], [Akhatov et al, 2005]. Indeed, figure-10 [Nigmatulin et al, 2005] shows a typical pressure distribution (where $r = R_c$ is at the edge and $r = 0$ is at the center of the bubble cluster during the bubble cluster implosion process. It can be seen that, due to a converging shock wave within the bubble cluster, there can be significant pressure intensification in the interior of the bubble cluster. This large local liquid pressure ($p_\ell > 1,000$ bar) will strongly compress the interior bubbles within the cluster, leading to conditions suitable for thermonuclear fusion [Lahey et al, 2005]. Moreover, during the expansion phase of the bubble cluster dynamics, coalescence of some of the interior bubbles is expected [Nigmatulin et al, 2005], and this will lead to the implosion of fairly large interior bubbles which produces more energetic implosions.

Typical HYDRO Code Predictions

Figure-11 presents some typical predictions of the conditions during the low Mach number stage of bubble dynamics. It can be seen that the bubbles within the bubble cluster grow when the incident liquid pressure (p_l) around them is negative and they begin to contract when the impressed acoustic incident pressure becomes positive. Due to the bubble cluster dynamics discussed above, we note significant pressure intensification during the bubble cluster implosion process. We also note that a lot of the vapor formed during the bubble expansion period is condensed during bubble implosion (i.e., until $T_{v_i} \geq T_{crit}$). This is important since condensation mitigates the vapor cushioning that occurs during the final phase of the implosion process. Finally, we see

that the vapor pressure is fairly constant (at p_{sat}) and the vapor temperature is essentially T_{pool} until the bubble implosion is well under way.

Figure-12 shows some typical results during the high Mach number stage of bubble implosion. The intensifying, inward moving, shock waves and the rebounding shock wave are clearly seen. Also, it is interesting to note that use of an ion thermal conductivity, Eqs. (8), leads to a precursory shock wave (compared to the case of constant thermal conductivity), however the peak temperatures, densities and pressures are not strongly affected by the energy losses related to thermal conduction within the vapor plasma.

As will be discussed shortly, the location where the vapor/plasma temperature and density are the greatest (and where thermonuclear fusion conditions may be most easily achieved) is not at the center of the bubble (r = 0) but at a nearby location, $r = r^* \sim 23$ nm, where the rebounding shock wave and the incoming compression wave interact. This compression process is fairly complicated as can be seen in figure-13 [Nigmatulin et al, 2005]. There are five stages to the compression process at $r = r^*$. The first stage ($t\text{-}t^* = -42$ to -15 μs) is a relatively slow, almost homobaric, expansion process during the (negative) time interval when the vapor density decreases. The second stage ($t\text{-}t^* = -15$ μs to 0.0) is a relatively slow compression during which the vapor density increases by a factor of ~ 32. This process is practically isentropic. The third stage involves a rapid compression due to the leading shock wave (Sh), where the density increases by a factor of ~ 17. The fourth stage occurs during a ~ 0.2 ps interval in which the density is further increased by a factor of ~ 5.9 by the incoming compression wave (similar to the famous Guderley [1942] problem). Finally, the fifth stage can be seen in figure-13, in which during ~ 0.05 ps the vapor/ plasma density increases by another factor of ~24 due to the interaction of the reflected leading shock wave and the incoming compression wave at r = r*.

The net effect of this rapid compression process is that the vapor/plasma density increases by a factor of ~ 77,000, a density which is more than ten times that of liquid acetone. Moreover, the local, instantaneous pressure is $\sim 10^{11}$ bar, the temperature is $> 10^8$ K, and the fluid velocity at r* reaches ~ 600 km/s; however these extreme conditions last for less than ~ 0.1 ps. Nevertheless, these conditions are suitable for thermonuclear D/D fusion.

Neutron Production

A HYDRO code evaluates the local, instantaneous thermal-hydraulic conditions within the bubble(s). In order to determine the local D/D neutron yield, we may use the neutron kinetics model presented by Gross [1984]:

$$J_n \equiv \frac{dn_n'''}{dt} = \frac{1}{2}\langle \sigma v \rangle \left(n_D'''\right)^2 \qquad (9)$$

where n_n''' is the local neutron concentration (n/m^3), n_D''' is the local concentration of deuterium ions (D/m^3), $<\sigma v>$ is the weighted cross section (m^3/s) for D/D fusion [Bosch & Hale, 1992], and the factor of two avoids double-counting fused deuterium ions. As can be seen in figure-14 the weighted cross section is strongly dependent on the vapor/plasma temperature, for both D/D and D/T fusion reactions (e.g., a change of about 12 orders of magnitude in the D/D fusion reaction when going from 10^6 K to 10^8 K). Also, we note that the D/T fusion reaction is several orders of magnitude more probable.

The total number of fusion neutrons (n_n) produced in each imploding bubble can be obtained by integrating Eq. (9) over the imploded bubble's volume (V_b) and the period of the acoustically-forced oscillations (1/f):

$$n_n = \int_{V_b} \int_0^{1/f} J_n dt dV = \int_0^R q(r) dr \qquad (10a)$$

where, q(r) characterizes the spatial distribution of the D/D fusion reactions, and because of the cylindrical geometry of the ORNL test section,

$$q(r) = 4\pi r^2 \int_0^{1/f} J_n(r,t) dt \qquad (10b)$$

Detailed HYDRO code evaluations [Nigmatulin et al, 2005] of q(r) and the distributions of the maximum vapor/plasma density and temperature are shown in figure-15. We see that the location of maximum D/D neutron production is at r* ~ 23 nm, and that endothermic "chemical" energy losses due to dissociation and ionization are not significant. Moreover, since the location of maximum fusion neutron production occurs at r>0, one does not need to resolve the near-singularity in temperature that occurs at the center of the bubble, thus it is not difficult to achieve nodal convergence of the numerical results.
For the conditions of the ORNL Sonofusion experiments [Taleyarkhan et al, 202; 2004] the HYDRO code predicts a 2.45 MeV D/D neutron yield of about
10 neutrons/implosion/bubble [Nigmatulin et al, 2005].

In order to do a global check of these results, we note that Eqs. (9) and (10a) imply:

$$n_n = \int_{V_b} \int_0^{1/f} \frac{1}{2} \langle \sigma v \rangle \left(n_D''' \right)^2 dt dV \qquad (11a)$$

which, using the mean value theorem, yields:

$$n_n \simeq \left(n_D''' \right)_\bullet^2 \langle \sigma v \rangle_\bullet R_\bullet^3 \Delta t_\bullet \qquad (11b)$$

Typical HYDRO code Sonofusion results at r=r* are [Nigmatulin et al, 2005]:

$$\left(n_D''' \right)_\bullet \sim 10^{30} \text{ D/m}^3 \left(@\rho_\bullet \sim 10^4 \text{ kg/m}^3 \right), \langle \sigma v \rangle_\bullet \sim 10^{-25} \text{ m}^3/\text{s} \left(@T_\bullet \sim 10^8 \text{ K} \right),$$

$R_{\bullet} \sim 60\text{nm}$ (see fig-15) and $\Delta t_{\bullet} \sim 1.0\,\text{ps}$, thus Eq. (11b) implies, $n_n \sim 10$ neutrons/implosion/bubble, which agrees with the more detailed HYDRO code predictions.

Due to localized pressure intensification and bubble coalescence within the bubble cluster, only about 15 bubbles are expected to experience energetic implosions. Also in the ORNL Sonofusion experiments, there were about 50 implosions/s of the bubble clusters which were nucleated by the PNG neutrons and, as can be seen in figure-6, there were about 50 "bounces" of the bubble cluster before the whole cycle was reinitiated again (i.e., the PNG fired again at 5 ms). Thus the HYDRO code results imply an average neutron production rate $(\dot{n}_n)$ of,

$$\dot{n}_n = (10)(15)(50)(50) \sim 4\times10^5 \,\text{neutrons/s} \qquad (12)$$

which is in very good agreement with the measured results [Taleyarkhan et al, 2002; 2004], [Nigmatulin et al, 2004].

Finally, it is interesting to compare HYDRO code results for typical SBSL experiments [Moss et al, 1994] with those for the ORNL Sonofusion experiments [Nigmatulin et al, 2005]. Table-I presents typical results. It can be seen that the maximum pressure and temperature (at r*) for the ORNL experiments are several orders of magnitude larger than for SBSL experiments, but the duration of these conditions (Δt_*) is less (i.e., the implosion during Sonofusion is faster and stronger than for SBSL). Thus we see that the experimental technique that was developed and used at ORNL produces results which are consistent with thermonuclear fusion, while the technique typically used in SBSL experiments is inherently unable to do so.

TABLE-I

TYPICAL HYDRO CODE RESULTS

Parameter	SBSL Results [Moss et al, 1994]	Sonofusion Results [Nigmatulin et al, 2005]
Δp_I	~1.0 bar	~15 bar
R_{core}	~2 nm	~60 nm
Δt_*	$\sim10^{-11}$ s	$\sim10^{-12}$ s
ρ_*	$\sim10^4$ kg/m^3	$\sim10^4$ kg/m^3
n'''_{D_*}	$\sim10^{30}$ D/m^3	$\sim10^{30}$ D/m^3
p_*	$\sim10^9$ bar	$\sim10^{11}$ bar
T_{i_*}	$\sim10^6$ K	$\sim10^8$ K
$\langle\sigma v\rangle_*$	$\sim10^{-37}$ m^3/s	$\sim10^{-25}$ m^3/s

Thus Eq. (11b) implies:

$$n_n \simeq \left(n_D'''\right)_*^2 \left\langle \sigma v \right\rangle_* R_{core}^3 \Delta t_* = \begin{cases} 10 \text{ neutrons / implosions / bubble, for } \textit{Sonofusion.} \\ 0.0, \text{ for } \textit{SBSL.} \end{cases}$$

The Effect of Liquid Pool Temperature

The mass flux $\left(\dot{m}_v''\right)$ of the vapor to $\left(\dot{m}_v'' < 0\right)$ or from $\left(\dot{m}_v'' > 0\right)$ the interface is given by the well known Hertz-Knudsen-Langmuir model:

$$\dot{m}_v'' = \frac{2\alpha}{(2-\alpha)}\left[\frac{p_{sat}(T_i) - p_{v_i}}{\sqrt{2\pi R_v T_i}}\right] \tag{13}$$

where α is the so-called accommodation (or phase change) coefficient. We note that the larger the value of α and the lower the vapor pressure, $p_{sat}(T_i)$, the larger the condensation rate (i.e., when $p_{v_i} > p_{sat}(T_i)$).

We can lower the saturation pressure of D-acetone by almost a factor of four by chilling the liquid pool from room temperature ($T_{L_0} = 293K$) to $T_{L_0} = 273K$. Moreover, hydrocarbons like D-acetone have a large accommodation coefficient (i.e., α ~ 1.0) compared to other candidate test liquids, for instance, heavy water, D_2O (i.e., α ~ 0.075).

Figure-16 shows the variations of vapor content (m_v) in the bubble and number of neutrons (n_n) produced with liquid pool temperature $\left(T_{L_0}\right)$. We can see that the neutron production rate increases significantly as the T_{L_0} is lowered and α is increased. In both situations this is due to the fact that there is less vapor mass (m_v) at the end of bubble collapse, which means that the cushioning during the final stages of the implosion process will be less and thus the vapor/plasma compression will be stronger. This seemingly paradoxical effect of liquid pool temperature has been verified experimentally [Taleyarkhan et al, 2002]. Indeed a statistically significant neutron yield was only measured for cavitation bubble implosions in a chilled (273 K) pool of well-degassed, cavitated liquid D-acetone.

Current Status and Future Directions

It is interesting to note that the Lawson criterion for D/D fusion ignition at 10^8 K [Gross, 1984], $\left(n_D'''\right)_\bullet \Delta t_\bullet \simeq 10^{22} s/m^3$, is about four orders of magnitude above what is predicted by the HYRDO code for the ORNL Sonofusion experiments,

$$\left(n_D'''\right)_\bullet \Delta t_\bullet = \left(10^{30} m^{-3}\right)\left(1\times 10^{-12} s\right) = 10^{18} s/m^3.$$

Thus in the ORNL experiments fusion "sparks" were experienced rather than a fusion burn. Moreover, the fusion neutron power produced in the ORNL experiments was about

seven orders of magnitude below break-even [Lahey et al, 2005]. Thus, the neutron yield will need to be significantly scaled-up before Sonofusion can be seriously considered for the purpose of net energy production. However, it may be possible to do so.

There is no reason to believe the D-acetone is the optimum test liquid, or that the ORNL experimental conditions were ideal. Indeed, a test liquid with a higher saturation temperature would have much better thermodynamic properties for applications in, for example, a Rankine cycle energy conversion system. Moreover, the D/T reaction (which yields 14.1 MeV neutrons), would produce an increase in neutron yield of about three orders of magnitude above that for D/D fusion, and due to the buildup of tritium during D/D fusion, this reaction would occur as time goes on.

Also, in order to scale-up the neutron yield, it appears that it may be possible to create a nuclear chain reaction between two adjoint acoustic anti-nodes that are externally excited 180˚ out-of-phase. That is, an external neutron source (e.g., PNG) could be used to cavitate a bubble cluster when the deuterated test liquid is under the maximum tension. After that, the scenario will be as shown in figure-2. In particular, when the initial implosion takes place 2.45 MeV neutrons will be produced and emitted in all directions (i.e., 4π). Some of these neutrons can interact with the acoustic anti-node of the adjacent test section, which at that point in time will be under maximum tension, thus causing a cavitation bubble cluster to form. If the conditions are appropriate a self-sustained nuclear chain reaction (i.e., criticality) might be created between the adjacent test sections.

The possibility of criticality can be appraised using the following formula:

$$S_2 = S_1\left[\frac{A}{4\pi R^2}\right]\eta e^{-\Sigma R} \equiv S_1 P\eta \qquad (14)$$

where, S_1 and S_2 are the D/D neutron source strengths at the acoustic anti-nodes in adjacent test sections 1 and 2, respectively; P is the probability that a D/D neutron produced in an acoustic antinode will interact with the adjacent antinode; A is the projected (spherical) area of the active acoustic antinode in each test section, η is the number of D/D neutrons produced per incident 2.45 MeV neutron on the antinode; R is the distance between the adjacent antinodes and Σ is the total macroscopic cross section for neutron attenuation in the materials between the adjacent acoustic antinodes.

Assuming the use of ORNL type test sections (see figure-3) and the validity of the experimental results [Taleyarkhan 2002; 2004] achieved there (i.e., $\eta \simeq 150$ neutrons), if the adjacent antinodes are a reasonable distance (R) apart we find that $p \simeq 1/\eta$, thus, $S_2 = S_1$, which implies that we can have a self-sustained nuclear chain reaction (i.e., criticality). This is obviously an exciting prospect since it implies a method by which a new type fusion reactor might be developed. Nevertheless, experimental confirmation is required.

CLOSURE

It is too early to fully understand the implications of Sonofusion technology. However, it appears that thermonuclear fusion occurs and is quite repeatable (i.e., *Sonofusion is a fact, not fiction*).

A low-cost, picosecond duration, pulsed neutron source might be useful for a wide range of biomedical, solid state physics and materials science or Sonochemistry applications. Also it appears to be a convenient way to parametrically study thermonuclear fusion processes and parameters (e.g., $<\sigma v>$. In addition, it may offer new opportunities for the production of helium-3 and/or tritium. Nevertheless, the "holy grail" of all fusion research is the development of a new, safe, environmentally friendly, way to produce electrical energy.

Much more research is required before it will become clear if Sonofusion can become a new energy source for mankind. Nevertheless, this exciting new technology appears to be inherently safe (e.g., there is no significant decay heat after reactor shut down) and, since the tritium produced will be burned in D/T reactions as fuel, Sonofusion should be much more environmentally friendly than other existing fusion/fossil energy sources. Moreover, the oceans contain enough deuterium to satisfy the earth's energy requirements for at least the next millennium [Lahey et al, 2005] if fusion energy becomes a reality.

Time will tell what the practical significance of Sonofusion technology may be, however it appears to be well worth the effort to pursue further research. It is hoped that this paper will stimulate multiphase thermal-hydraulic researchers around the world to work on Sonofusion technology so that its full potential may be realized.

REFERENCES

Akhatov, I.S., Gumerov, N., Ohl, C.D., Parlitz, V., Lauterborn, W. (1997) "The Role of Surface Tension in Stable Single Bubble Sonoluminescence," *Phys. Rev. Lett*, **78**, 227.

Akhatov, I.S., Nigmatulin, R.I., Lahey, R.T., Jr. (2005) "The Analysis of Linear and Nonlinear Bubble Cluster Dynamics," in press, *Multiphase Science & Technology*.

Bosch, H.-S. and Hale, G.M., (1992) "Improved formulas for fusion cross-sections and thermal reactivities," *Nuclear Fusion*, **32**, 61.

Brennen, C.E. (1995) "Cavitation and Bubble Dynamics," Oxford University Press, New York.

Camara, C., Putterman, S., Kirilov, E. (2004) "Sonluminescence From a Single Bubble Driven at 1 Megahertz," *Phys. Rev. Lett*., **92**(12), 124001-1.

Crum, L.A. (1994) "Sonoluminescence, Sonochemistry, and Sonophysics," *J. Acoust. Soc. Am.*, **95**(1), 559.

Frenzel, J., Schultes, H. (1934) "Luminescenz in ultraschallbeschickten wasser," Kurze Mitteilung, *Zeit fur* Phys. Chem, **B27**, 421.

Gross. R.A. (1984) "Fusion Energy," John Wiley & Sons, New York.

Guderley, G. (1942) "Starke Kugelige und Zylindresche Verdichtungsstobe in der nahe des Kugelmittelpunktes der Zylinderachse," *Luftfahrtforschung*, **19**.

Knoll, G.F. (1989) "Radiation Detection and Measurement," Wiley, New York.

Lahey, R.T., Jr., Taleyarkhan, R.P., Nigmatulin, R.I., Akhatov, I.S. (2005) "Sonoluminescence and the Search for Sonofusion," *Advances in Heat Transfer*, **39**, Academic Press.

Lauterborn, W., Kurz, T., Mettin, R., Ohl, C.D. (1999) "Experimental and Theoretical Bubble Dynamics," *Advances in Chemical Physics*, **110**, 295.

Margulis, M.A. (2000) "Sonoluminescence," *Phys. Sci. Advances*, **170**(3), 263 (In Russian).

Marinesco, N., Trillat, J.J. (1933) "Chimie physique – action des ultrasons sur les plaques photographiques," *Comptes Rendes Acad. Sci. Paris*, **196**, 858.

Moss, W.C., Clarke, D.B., White, J.W. and Young, D.A. (1994) "Hydrodynamic Simulations of Bubble Collapse and Picosecond Sonoluminescence," *Phys. of Fluids*, **6**(9), 2979.

Moss, W.C., Clarke, D.B., White, J.W., Young, D.A. (1996) "Sonoluminescence and the Prospects for Table-Top Micro-Thermonuclear Fusion," *Phys. Lett A* **211**, 69.

Moss, W.C., Clarke, D.B. and Young, D.A. (1997) "Calculated Pulse Widths and Spectra of a Single Sonoluminescing Bubble," *Science*, **276**, 1398.

Mullins, J. (2005) "Pop!," *New Scientist*, **22**, 38.

Nagrath, S., Jansen, K.E., Lahey, R.T., Jr., Akhatov, I.S. (2005) "Hydrodynamic Simulation of Air Bubble Implosion Using a FEM-based Level Set Approach," submitted for publication, *J. Computational Physics*.

Nigmatulin, R.I., Akhatov, I.S., Vakhitova, N.K., and Lahey, R.T., Jr. (2000) "On the Forced Oscillations of a Small Gas Bubble in a Spherical Liquid-Filled Flask," *J. Fluid Mech*, **414**, 47.

Nigmatulin, R.I., Taleyarkhan, R.P., Lahey, R.T., Jr., (2004) "The Evidence for Nuclear Emissions During Acoustic Cavitation Revisited," *J. Power & Energy*, **128(A)**, 345.

Nigmatulin, R.I., Akhatov, I., Bolotnova, R.K., Topolnikov, A.S., Vakhitova, N.K., Lahey, R.T., Jr., and Taleyarkhan, R.P., (2005) "The Theory of Supercompression of Vapor Bubbles and Nano-Scale Thermonuclear Fusion," submitted for publication, *Physics of Fluids*.

Putterman, S.J., Weninger, K.R. (2000) "Sonoluminescence: How Bubbles Turn Sound Into Light," *Annu. Rev. Fluid Mech*., **32**, 445.

Taleyarkhan, R.P., Cho, J.S., West, C.D., Lahey, R.T., Jr., Nigmatulin, R.I., and Block, R.C. (2002) "Evidence for Nuclear Emissions During Acoustic Cavitation," *Science*, **295**, 1868.

Taleyarkhan, R.P., West, C., Cho, J.S., Lahey, R.T., Jr., Nigmatulin, R.I., Block, R.C. (2004) "Additional Evidence of Nuclear Emissions During Acoustic Cavitation," *Phys. Rev. E.*, **69**.

Taleyarkhan, R.P., Lahey, R.T., Jr., Nigmatulin, R.I. (2005) "Bubble Nuclear Fusion Technology – Status and Challenges," in press, *Multiphase Science & Technology*.

Tien, C.L., Majumdar, A. and Gerner, F.M. – eds. (1998) "Microscale Energy Transport," Taylor & Francis, Washington, D.C.

Trunin, R.F., Zhernokletov, M.V., Kuznetsov, N.F., Radchenko, O.A., Sichevskaya, N.V., and Shutov, V.V. (1992) "Compression of Liquid Organic Substances in Shock Waves," *Khimicheskaya Fizika*, **11**, 424 (in Russian).

West, C. (1967) "Cavitation Nucleation by Energetic Particles," Topical Report – Electronics and Applied Physics Division, AERE, Harwell, Berkshire, UK.

West, C.D., Howlet, R. (1967) "Timing of Sonoluminescence Flash," *Nature*, 215, 727.

West, C.D. Howlet, R. (1968) "Some Experiments on Ultrasonic Cavitation using a Pulsed Neutron Source," *Brit. J. Appl. Phys*., **1**, 247.

Young, F.R. (2004) "Sonoluminescence," CRC Press.

Zeldovich, Y.B., Raizer, Y.P. (1966) "Physics of Shock Waves and High-Temperature Hydrodynamic Phenomena," Academic Press.

Zimakov, P.V.D., (1934) " On Some Water Solutions in Electromagnetic Fields of High Frequency", *R. Acad. Sci. – USSR*, **3**, 450 (In Russian).

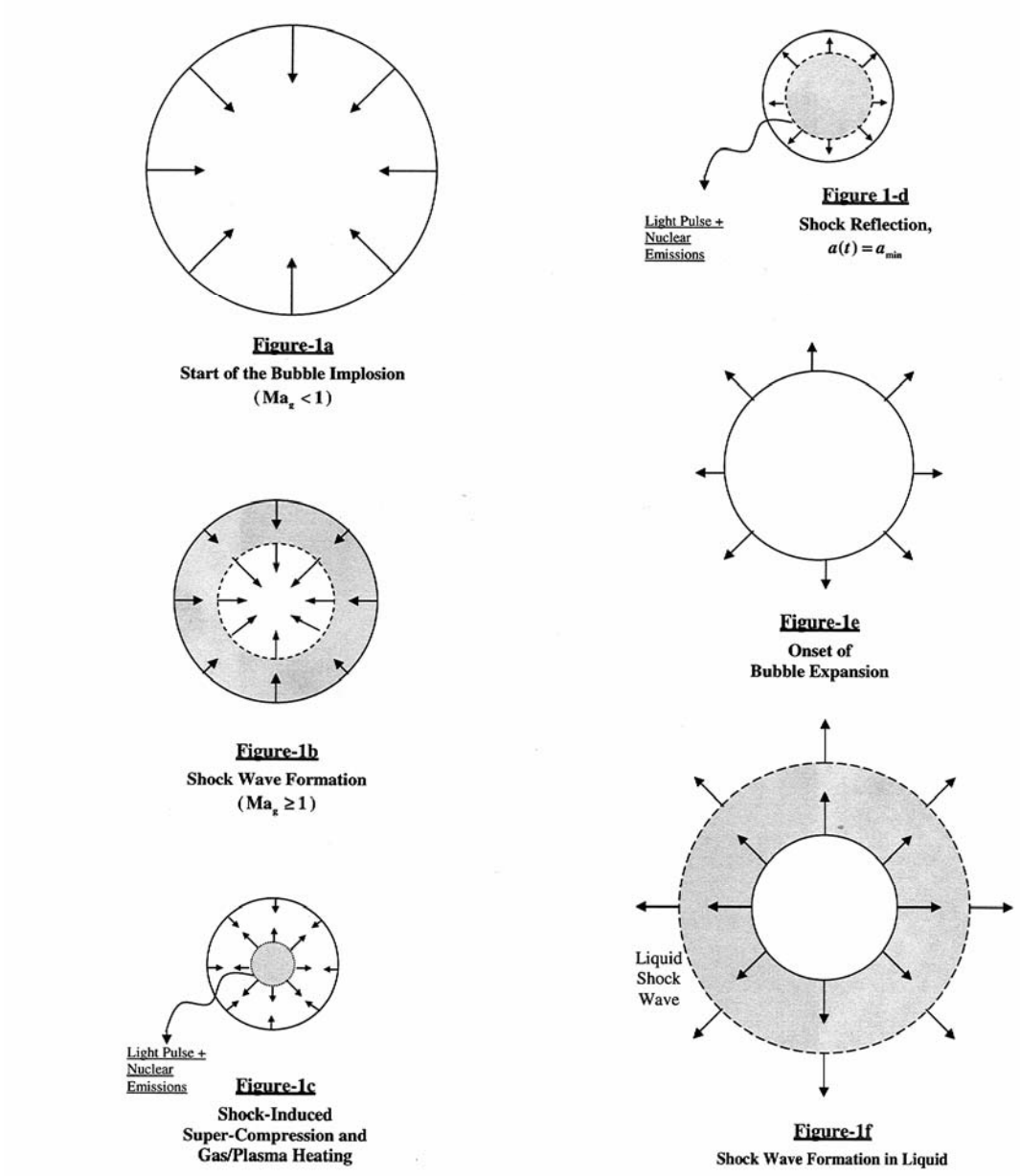

Fig. 1. Schematic of Sonoluminescence and Sonofusion phenomena.

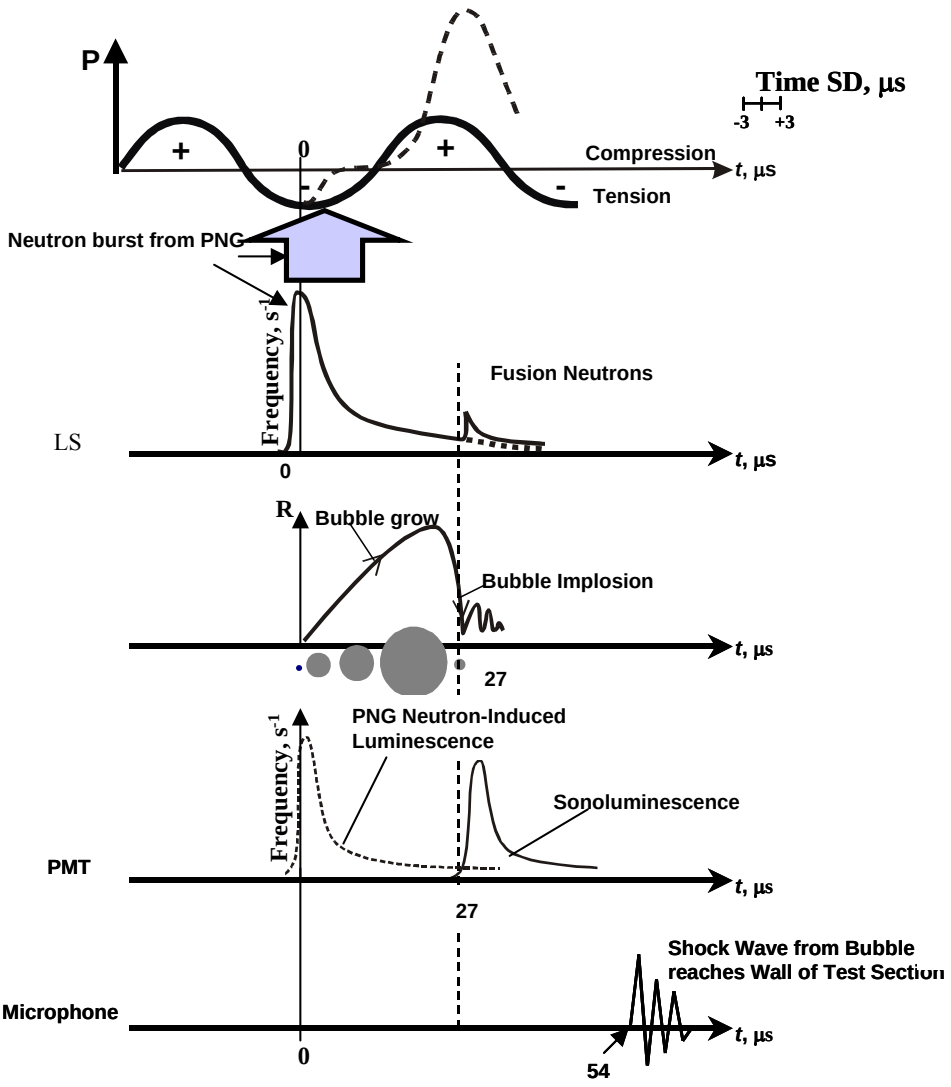

Fig. 2 Schematic sequence of events during typical Sonofusion experiments

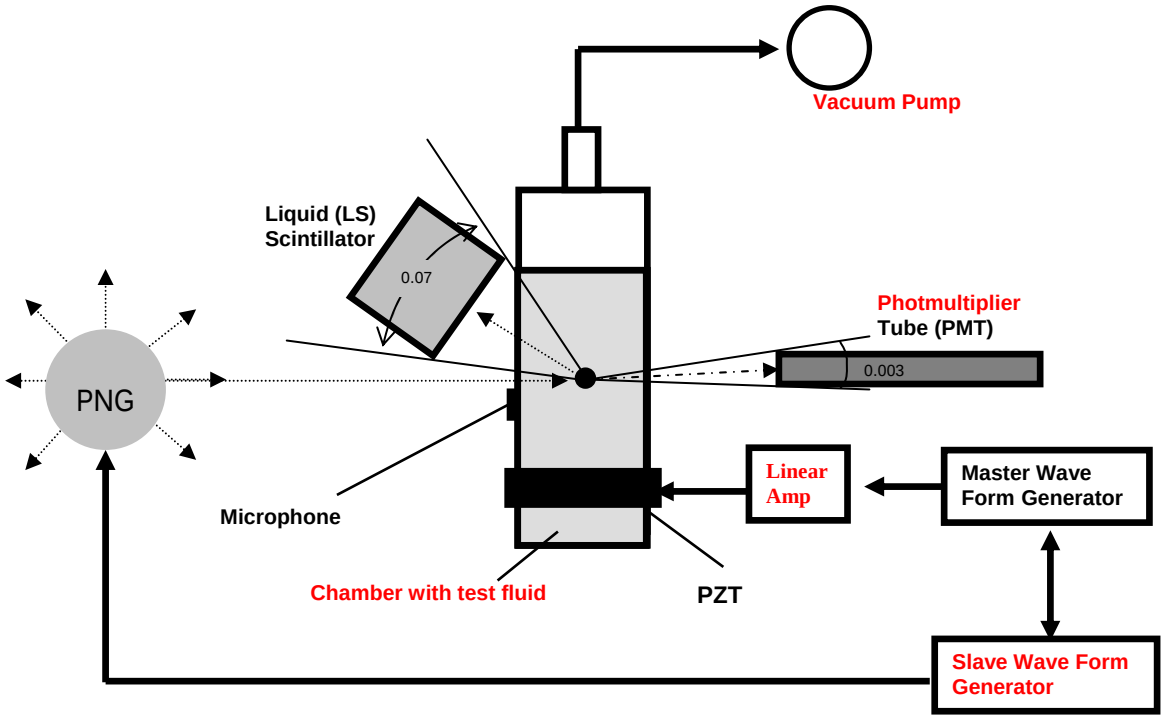

Fig. 3 Typical Experimental Configuration [Taleyarkhan et al, 2002; 2004].

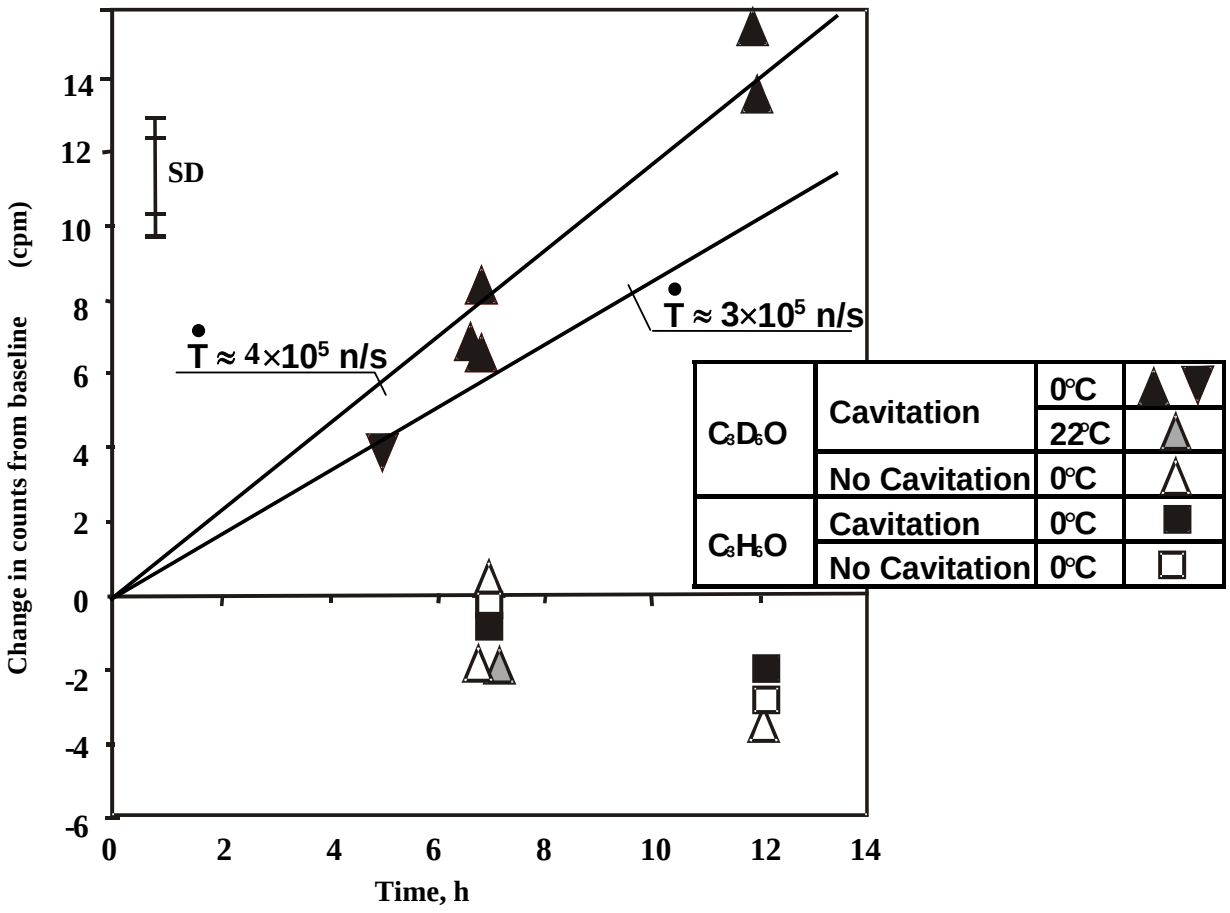

Fig. 4 ORNL Tritium data [Taleyarkhan et al, 2002;2004]

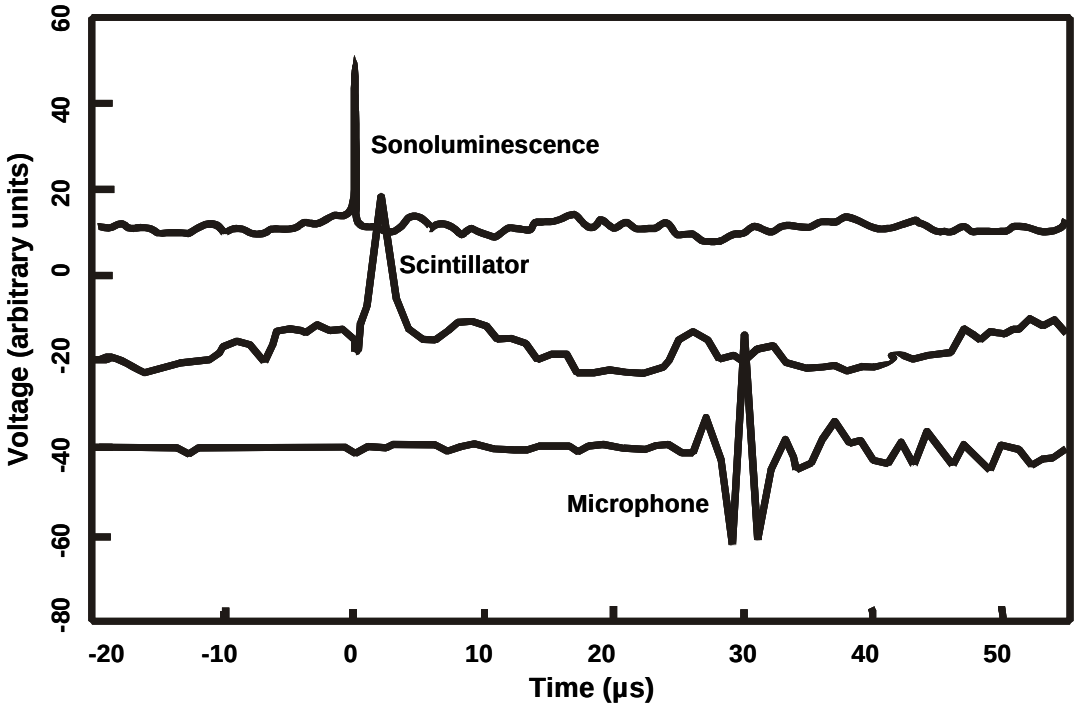

Fig. 5 Coincident light/neutron emissions and subsequent shock wave signals for D-acetone at 0˚C [Taleyarkhan et al, 2002].

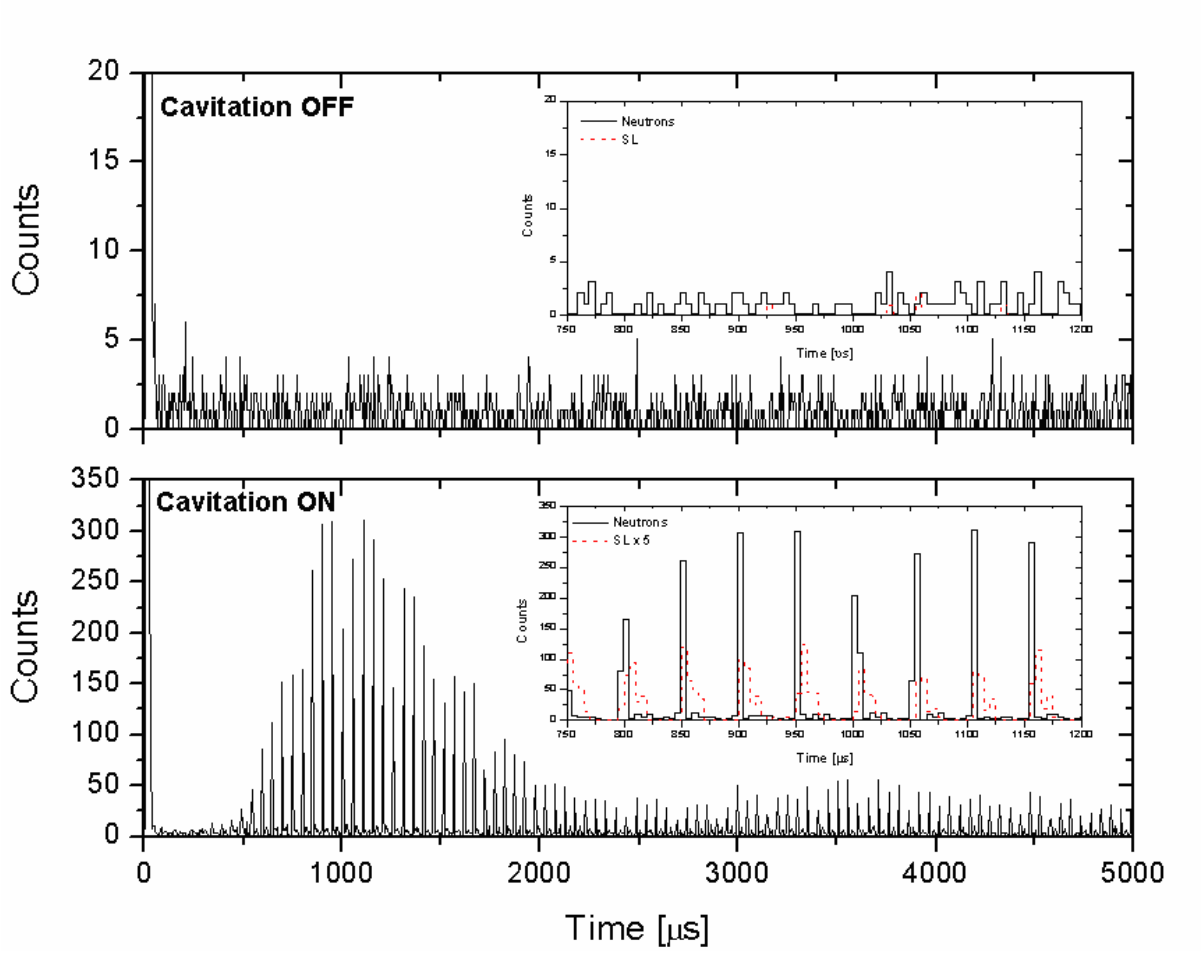

Fig. 6 Data for chilled (0˚C) irradiated D-acetone (C_3D_60) with and without cavitation [Taleyarkhan et al, 2004]

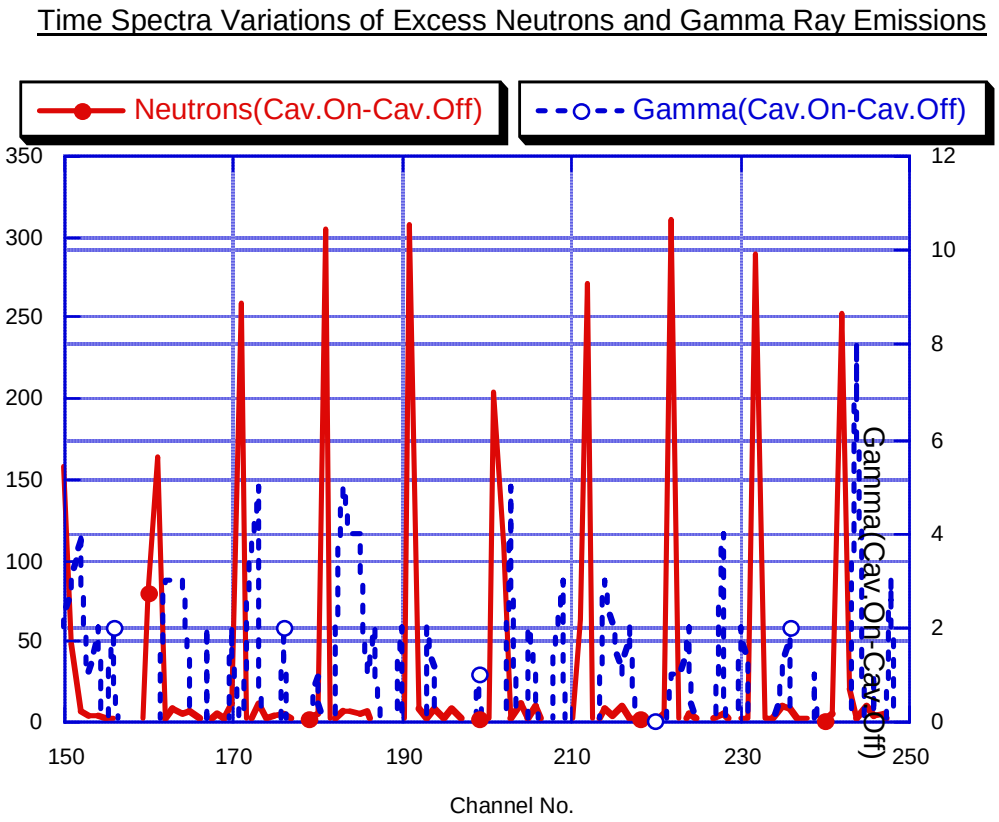

Fig. 7 Time variation of neutron and gamma emissions during Sonofusion [Taleyarkhan et al, 2005]

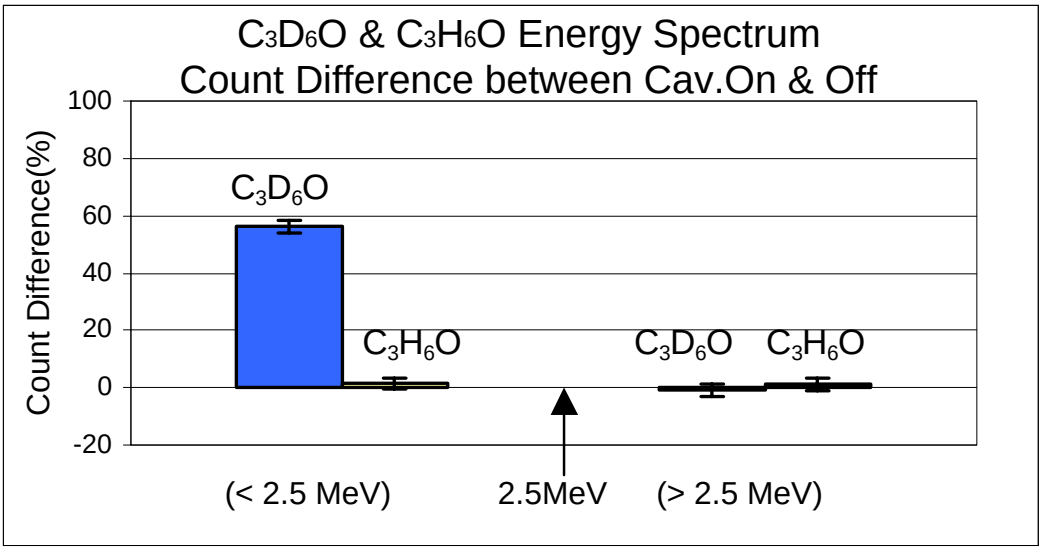

Fig. 8 Changes in neutron counts below and above 2.5 MeV for tests with C_3D_6O and C_3H_6O at ~0˚C,with and without cavitation [Taleyarkhan et al, 2004].

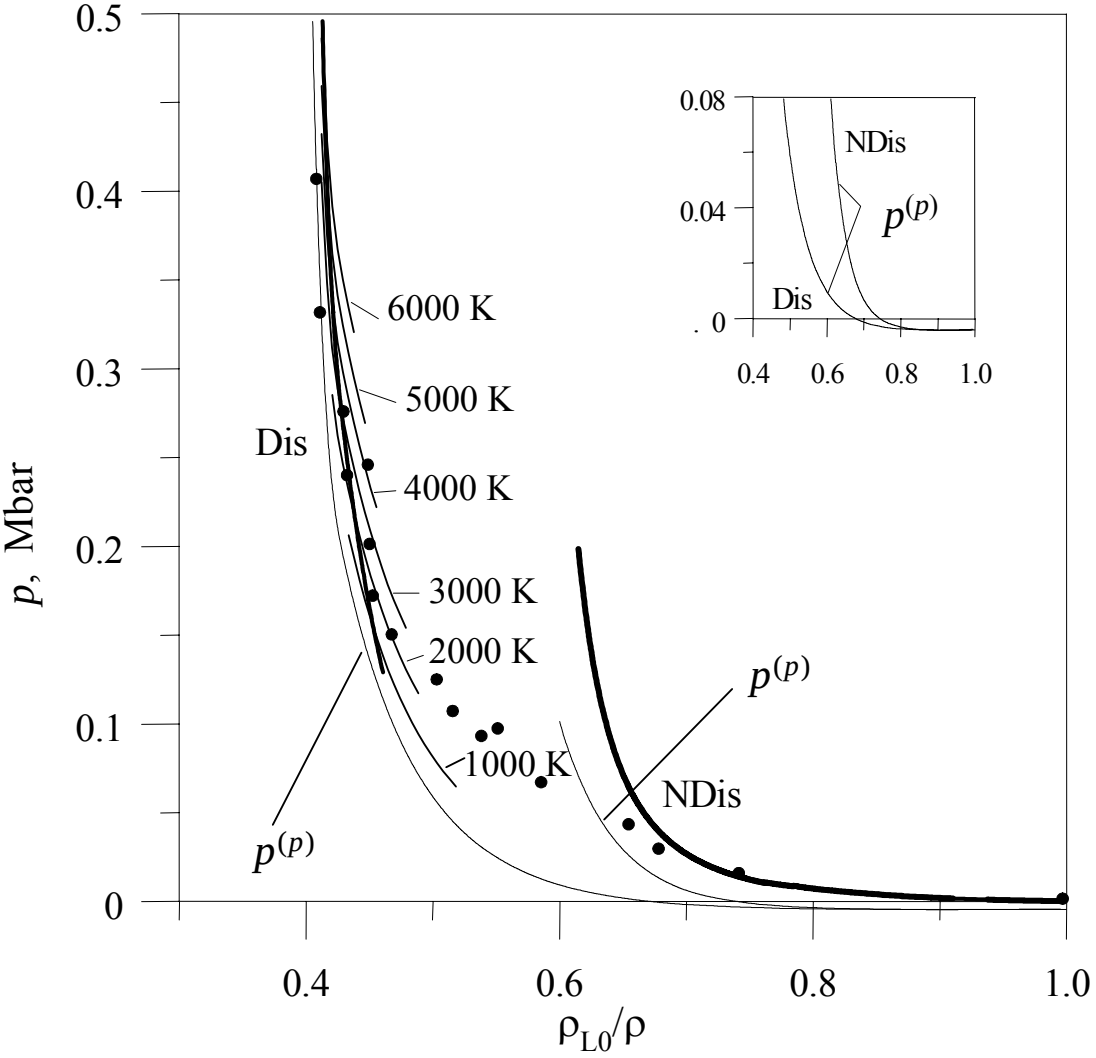

Fig. 9 Comparison of Equation of State with Data of Trunin et al [1992]

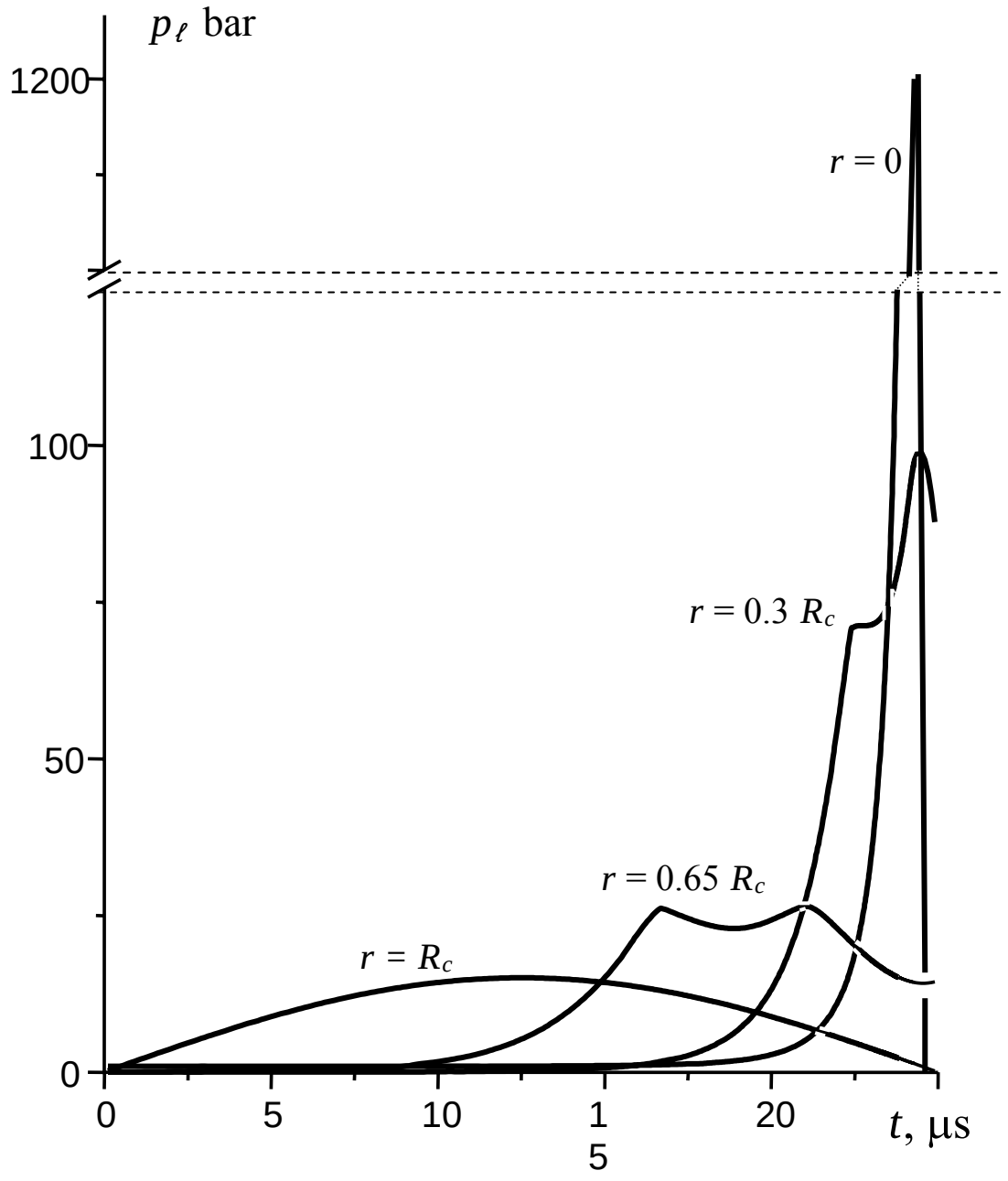

Fig. 10 The evolution of liquid pressure within an imploding bubble cluster of radius R_c at various radial positions (r) for: 1,000 bubbles/cluster, R_o = 300 μm, α_{v_o} = 0.04, and Δp_I = 15 bar.

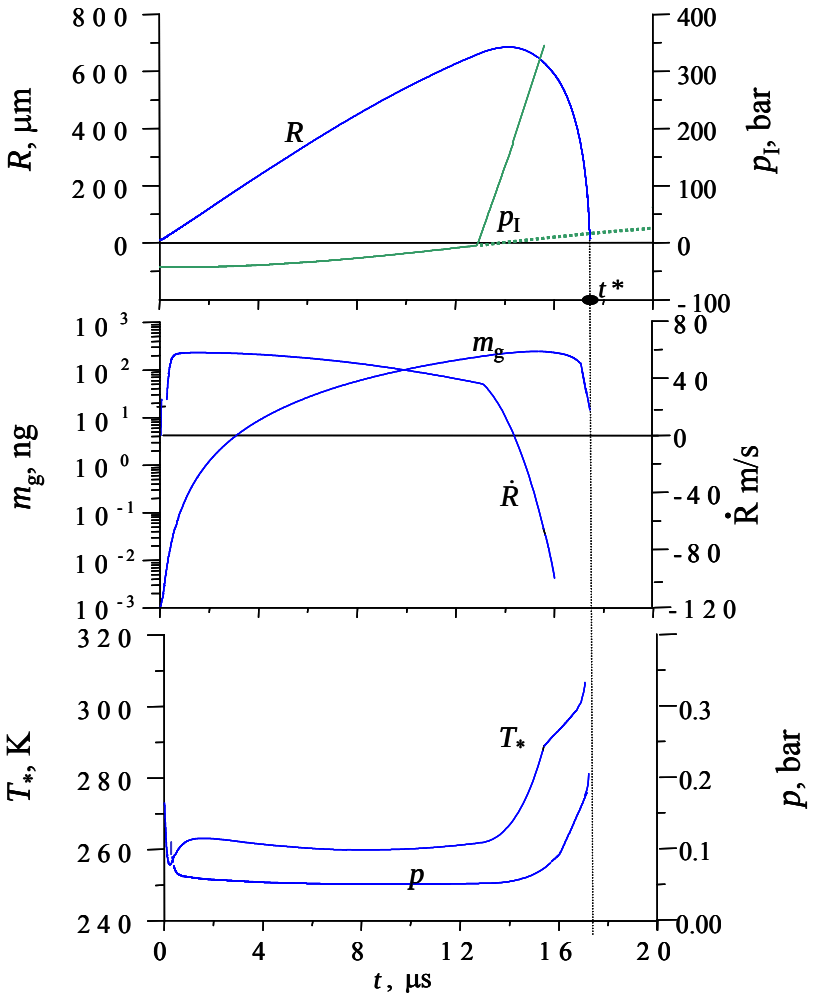

Fig. 11 Low Mach Number Stage of Bubble Dynamics

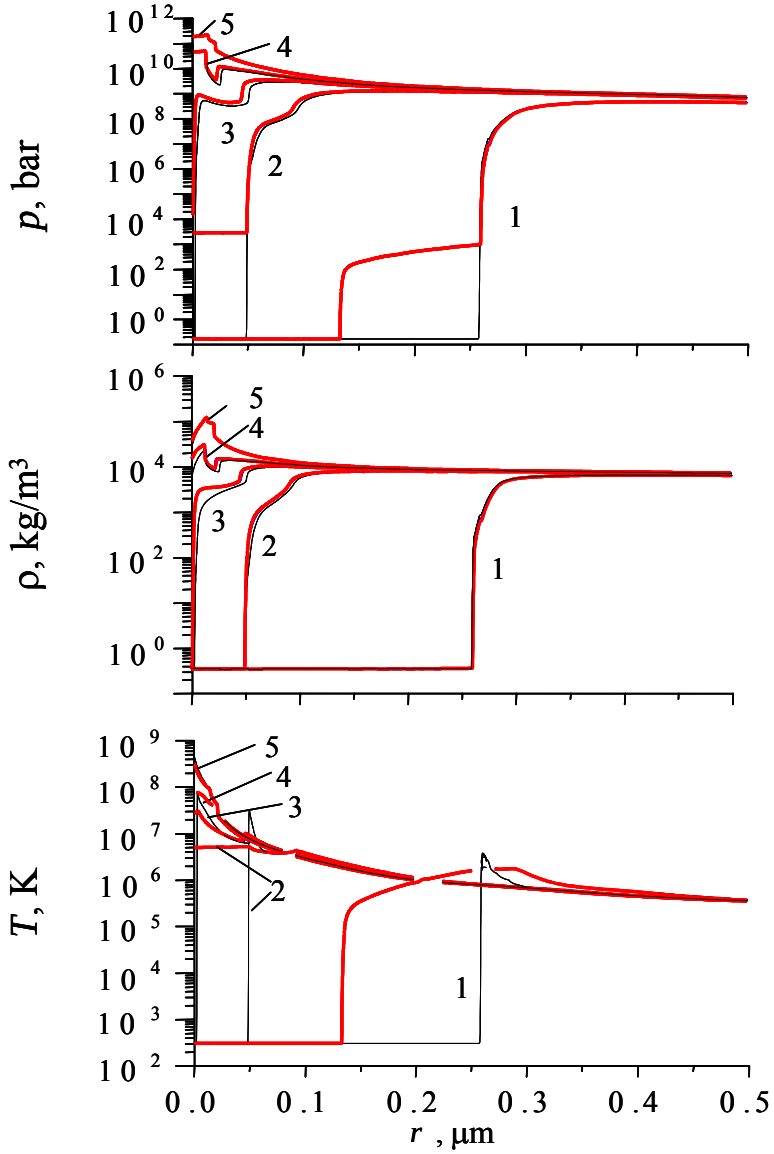

Fig. 12 Shock wave propagation and cumulation within a bubble during the high Mach number stage of bubble implosion (thick red lines use Eqs. (8) and thin lines use a constant thermal conductivity). The numbers indicate the spatial distributions at relative times: $t_1 \equiv 0.0$, $t_2 = 0.61$ ps, $t_3 = 0.68$ ps, $t_4 = 0.72$ ps and $t_5 = 0.76$ ps.

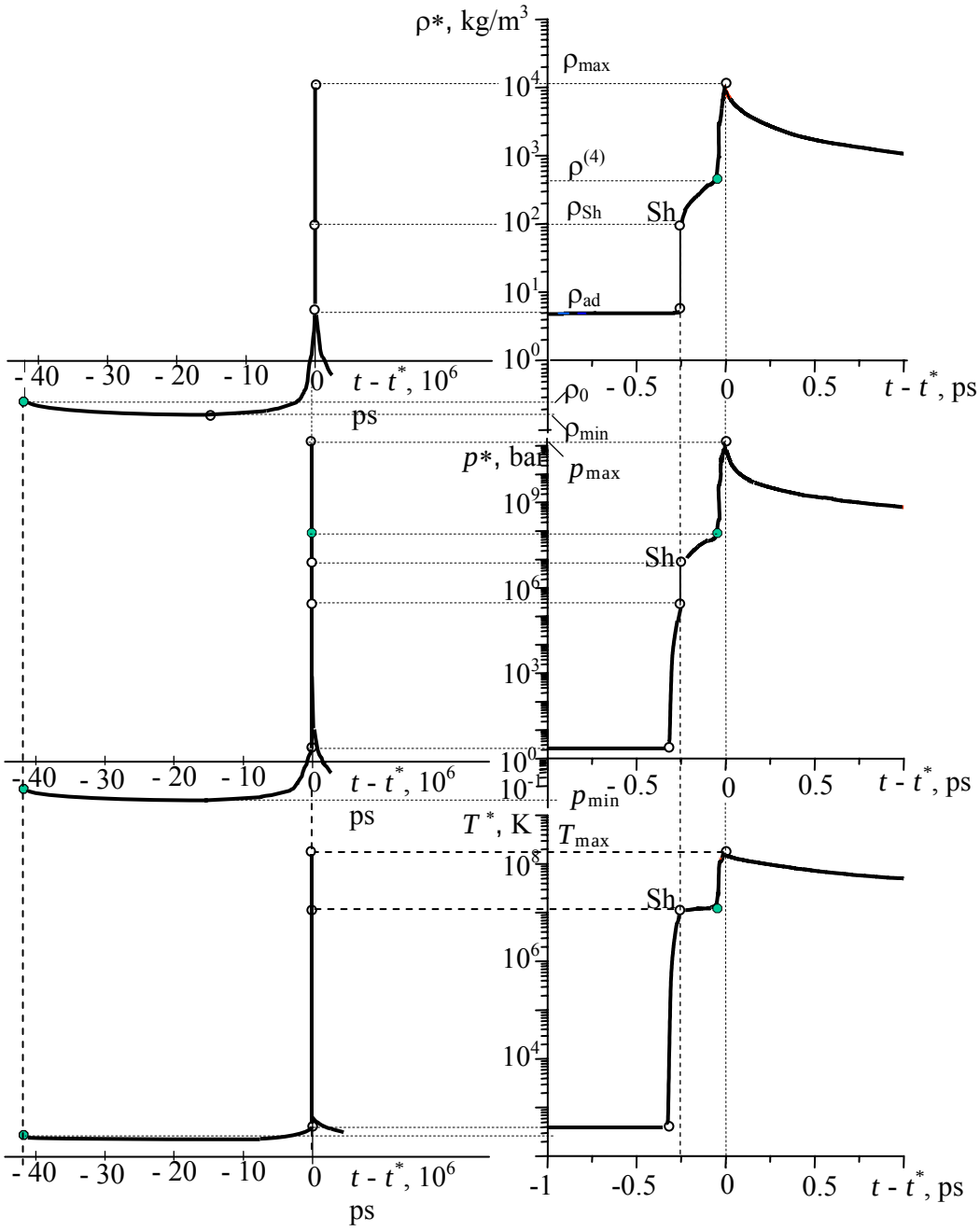

Fig. 13 The temporal distributions of vapor/plasma density (ρ), pressure (p), and temperature (T) at r = r* during the final high Mach number stage of bubble implosion.

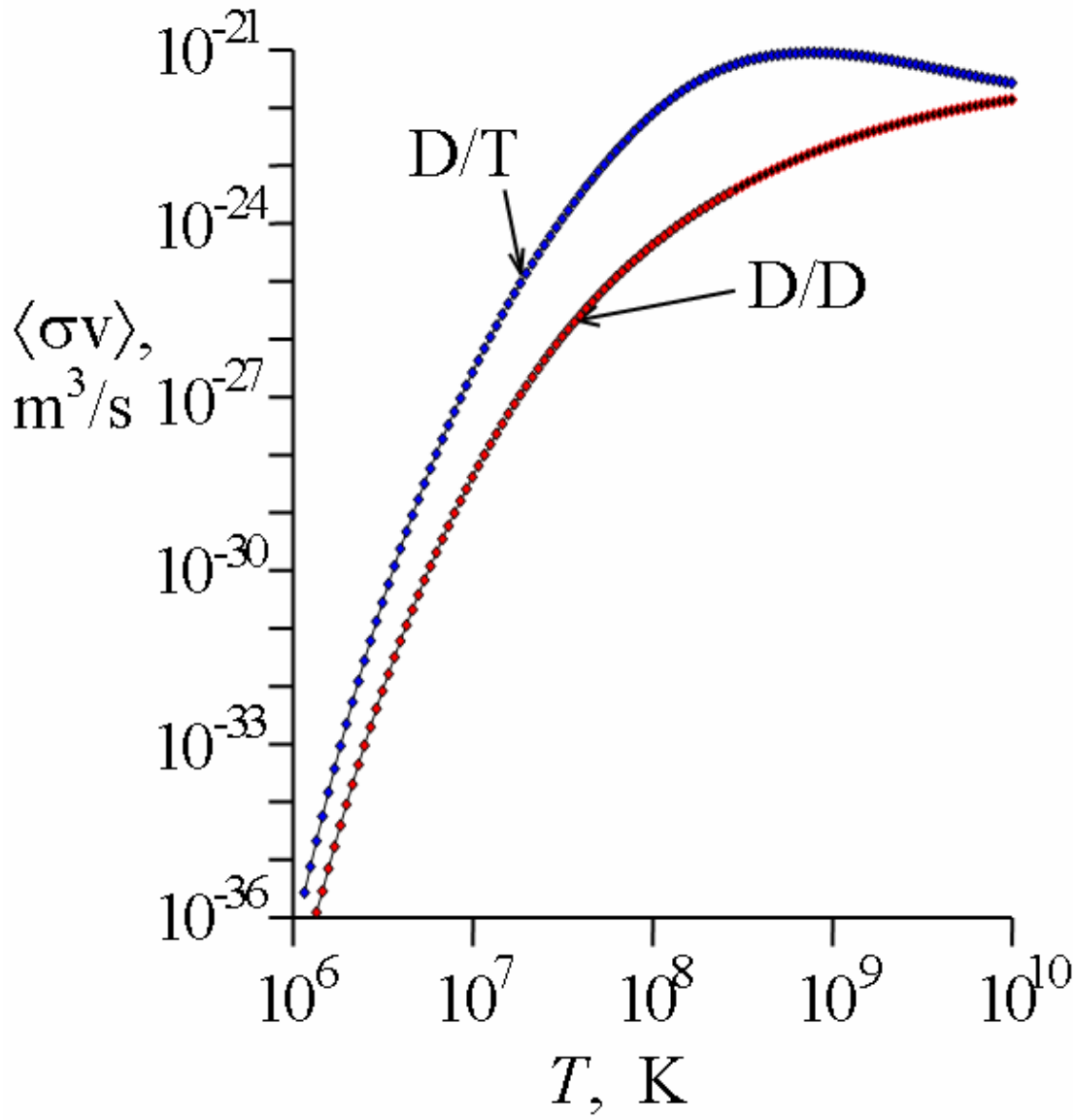

Fig. 14 Variation of weighted fusion cross-sections with vapor/plasma temperature

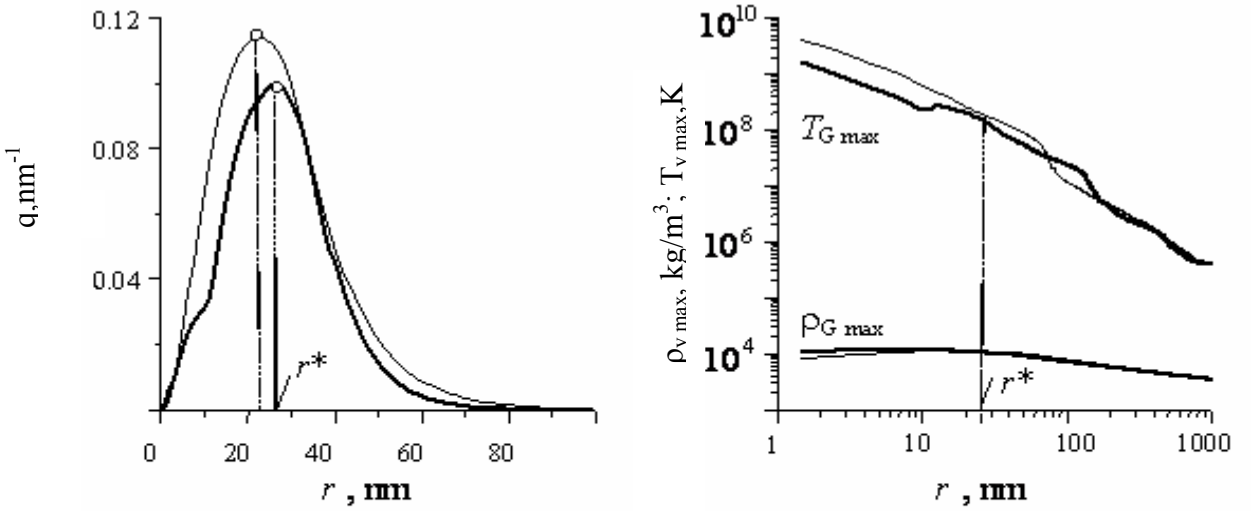

Fig. 15 The maximum neutron production distribution (q), and maximum vapor/plasma temperatures ($T_{v_{max}}$) and densities ($\rho_{v_{max}}$) with (heavy lines) and without (thin lines) endothermic "chemical" reaction energy losses from the dissociation and ionization of C_3D_6O molecules.

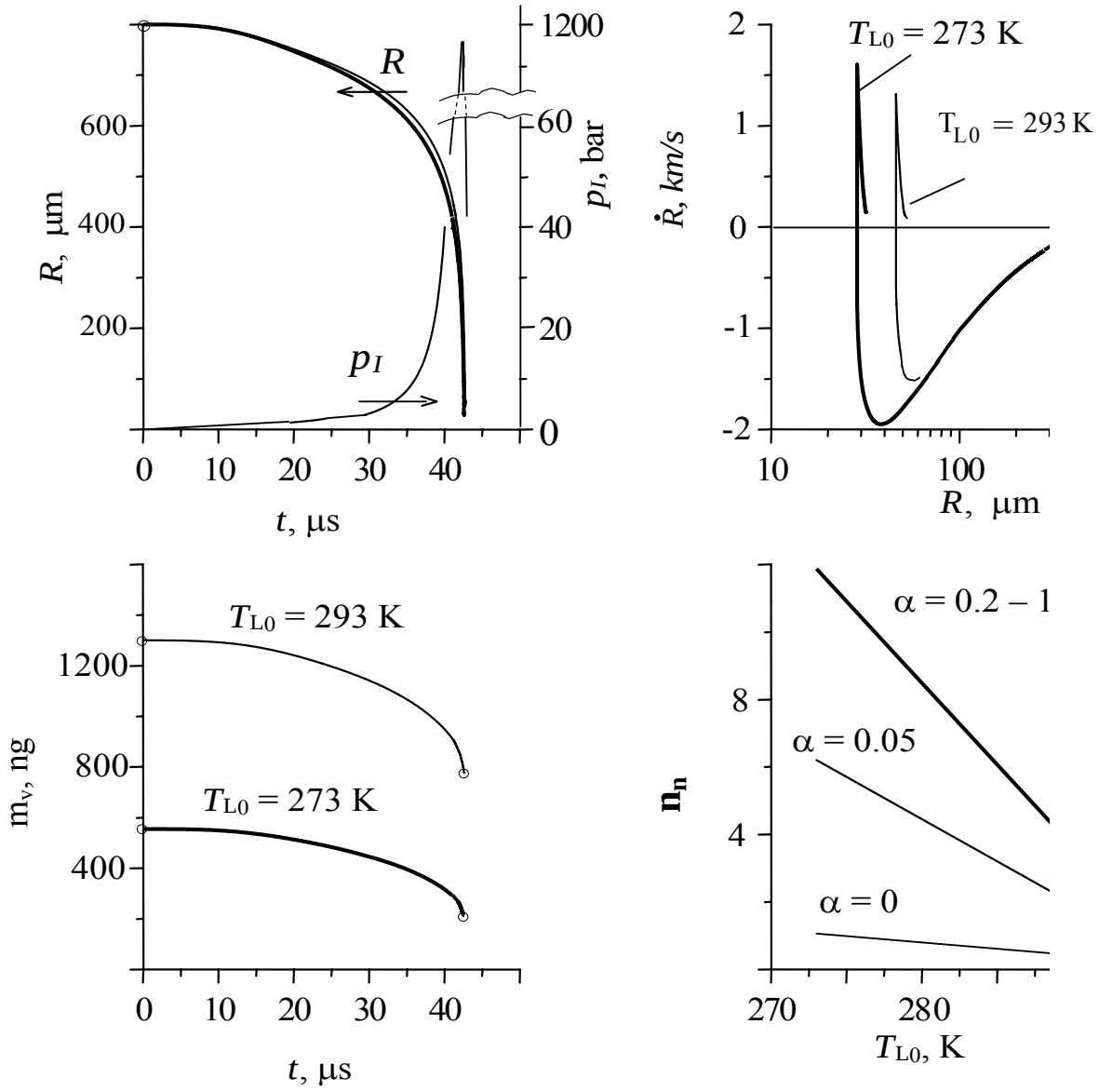

Fig. 16 The influence of liquid pool temperature (T_{L0}) and accommodation coefficient (α) on D/D neutron production (n_n), vapor mass (m_v), bubble radius (R) and interfacial velocity ($\dot{R}$)